Buckling prediction of composite lattice sandwich cylinders (CLSC) through the vibration correlation technique (VCT): Numerical assessment with experimental and analytical verification

Davoud Shahgholian-Ghahfarokhi, Gholamhossein Rahimi, Gholamhossein Liaghat, Richard Degenhardt, Felipe Franzoni

PII: S1359-8368(20)33302-3

DOI: https://doi.org/10.1016/j.compositesb.2020.108252

Reference: JCOMB 108252

To appear in: *Composites Part B*

Received Date: 10 April 2020

Revised Date: 12 June 2020

Accepted Date: 23 June 2020

Please cite this article as: Shahgholian-Ghahfarokhi D, Rahimi G, Liaghat G, Degenhardt R, Franzoni F, Buckling prediction of composite lattice sandwich cylinders (CLSC) through the vibration correlation technique (VCT): Numerical assessment with experimental and analytical verification, *Composites Part B*, https://doi.org/10.1016/j.compositesb.2020.108252.

CRediT authorship contribution statement

Davoud Shahgholian-Ghahfarokhi:

Conceptualization, Methodology, Software, Validation, Investigation, Writing - original draft, Writing - review & editing.

Gholamhossein Rahimi:

Conceptualization, Writing - review & editing, Supervision, Project administration.

Gholamhossein Liaghat:

Conceptualization,Writing - review & editing, Supervision, Project administration.

Richard Degenhardt:

Conceptualization, Methodology, Writing - review & editing, Supervision.

Felipe Franzoni:

Writing - review& editing, Investigation.

Buckling prediction of composite lattice sandwich cylinders (CLSC) through the vibration correlation technique (VCT): Numerical assessment with experimental and analytical verification

Davoud Shahgholian-Ghahfarokhi [a,*], Gholamhossein Rahimi [a], Gholamhossein Liaghat [a,b], Richard Degenhardt [c,d,e], Felipe Franzoni [c,d]

[a] *Department of Mechanical Engineering, Tarbiat Modares University, Tehran, Iran*

[b] *Department of Mechanical Engineering, Kingston University, London, United Kingdom*

[c] *DLR, Institute of Composite Structures and Adaptive Systems, Braunschweig, Germany*

[d] *University of Bremen, Faserinstitut Bremen e.V., Bremen, Germany*

[e] *PFH, Private University of Applied Sciences Göttingen, Composite Engineering, Campus Stade, Stade, Germany*

*Corresponding Author E-mail: D.Shahgholian@modares.ac.ir

Tel: +982182883356

Fax: +982182884909

Abstract

One of the best nondestructive techniques to evaluate the buckling behavior of imperfection-sensitive structures is the vibration correlation technique (VCT). This paper presents an analytical formulation for the free vibration of axially loaded composite lattice sandwich cylinders (CLSC) and numerical and experimental validations of the VCT applied to such structures. From an analytical point of view, the equations are obtained through the Rayleigh-Ritz method considering first-order shear deformation theory (FSDT). For the numerical verification of the VCT, three types of linear and nonlinear finite element analyses are performed. At first, numerical results for the critical buckling load and the first natural frequency at different load levels are compared with the corresponding analytical ones, validating the numerical models. Then, the numerical models are extended considering geometric nonlinearities and imperfection to simulate the variation of the first natural frequency of vibration with the applied load. As well, a nonlinear buckling analysis is also performed using the Riks method for a better comparison of the VCT results. In the last section, four specimens are fabricated using a new rubber mold and a filament winding machine. Additionally, the experimental buckling test is carried out, verifying the results of the VCT approach. The results demonstrate that the maximum difference between the estimated buckling load using the VCT approach and the corresponding nonlinear and experimental buckling loads is less than 5%, being the VCT result more accurate than the numerical one. Moreover, the proposed VCT provided a good estimation of the buckling load of the CLSC, considering a maximum load level of at least 62.1% of the experimental buckling load.

Keywords:

Buckling, Vibration Correlation Technique (VCT), composite lattice sandwich cylinders (CLSC), Analytical approach, Finite element analysis, Experimental test, Imperfection-sensitive structures

1. Introduction

Putting a core material between two stiffening skins is a good idea to increase the structural stiffness in comparison with a conventional solution such as increasing the thickness. Composite sandwich structures are fabricated from inner skin, core, and outer skin. According to industrial applications, the core can be designed homogeneous or non-homogeneous with various materials. Composite lattice sandwich cylinders (CLSC) are one of the most efficient types of sandwich structures due to their high stiffness-to-weight ratio, high breakdown strength, and lower damage growth, which have many applications in the aerospace [1-3], and offshore [4, 5] industries. Composite lattice sandwich cylinders are discontinuous structures established from skins, stiffeners, and periodic cells. Hence, they are highly efficient and widely used in various aerospace applications such as rocket interstates, payload adapters for launchers, and fuselage components for airplane [6]. Considering such applications, these structures are usually under axial load, lateral pressure, or both. In this context, the buckling analysis plays a fundamental role in the designing procedure of them, and it is one of the most important failure analyses.

Many researchers have been focused on buckling and vibrational analyses of CLSC. Fan et al. [7] proposed an efficient method to fabricate carbon fiber-reinforced composite (CFRC) sandwich shell with filament winding and twice co-curing processes. It was shown that the CLSC has better strength in comparison with a stiffened cylinder. A new mold was designed with foam material to fabricate filament wound grid-stiffened composite cylindrical structures by Buragohain and Velmurugan [8]. It was shown that CLSC has better mechanical performance rather than an unstiffened shell (with skin only) and a lattice cylinder (with ribs only). Vasiliev et al. [9] explained the lattice sandwich structure (LSC) application in the Russian aerospace industry. They provided material properties and fabrication method and design methods of LSC. Sun et al. [10] provided an analytical method to investigate the buckling behavior of the CFRC sandwich shell with a grid core under uniaxial compression. Five failure modes were introduced in this paper for composite sandwich cylinders. It should be noted that the analytical method has been developed for an isotropic shell. Improved manufacturing methods and new designs of the CFRC sandwich shell were presented by Chen et al. [11]. They concluded that skin and core thicknesses should be well balanced to have high-grade mechanical properties. Free vibration experiments were accomplished to investigate the mechanical behaviors of CFRC sandwich shells with lattice core. It was shown that the LSC has a higher fundamental frequency and could be considered lighter in different astronautic applications. Han et al. [12] investigated the free vibration behaviors of the CFRC lattice-core sandwich shell with the attached mass. It was shown that attached mass reduces a natural frequency. Loptain et al. [13] introduced a finite element model (FEM) to evaluate the dynamic and buckling behavior of composite lattice cylindrical shells with elliptical cross-sections. The results corroborated that the mentioned FEM is appropriate for desining composite tubular bodies of spacecraft. Jiang et al. [14] designed and fabricated a composite orthogrid sandwich cylinder using interlocking and filament winding methods, calculating the load-carrying capacity and natural frequencies of the structure. In another work, the multi-failure criteria for a composite orthogrid sandwich cylinder were

presented by them [15]. An analytical study was performed to calculate the failure mode of CLSC under various fundamental loads by Sun et al. [16]. For the failure modes introduced in Ref. [10], the load-carrying capacity of the structure was calculated theoretically and numerically. They presented a failure mode map that is useful for designing CLSC. Recently, Shahgholian-Ghahfarokhi and Rahimi [17, 18] presented a new analytical approach to study the buckling behavior of CLSC under uniaxial compression. The equations were obtained using the smear stiffener method, classical laminate theory (CLT), and first-order shear deformation theory (FSDT). It was shown that the proposed analytical method could predict the linear buckling load of the structure with high accuracy and low computational cost. In another work[19], they performed a sensitivity analysis of the free vibration of sandwich shells with lattice cores.

According to the above literature review, it can be seen that there are many methods to predict and calculate the buckling behavior of CLSC. From experimental, computational, and economic costs point of view, many of these methods present limited results. Thus, there is a great interest in the development and validation of nondestructive tests (NDT) to calculate the buckling load of such structures from the pre-buckling stage. The first NDT suggestion based on the correlation with the vibration response was given by Sommerfeld [20] in 1905 for conventional structure like columns. One of the best NDT methods to calculate the buckling load of an imperfection-sensitive thin-walled structure is the Vibration Correlation Technique (VCT). According to the VCT, the natural frequencies of a loaded structure are measured at the unloaded condition. In a second stage, the vibration frequency variation related to the increase of the axially applied load is recorded, without actually reaching the instability point. In the final stage, the curve fitting is performed between recorded natural frequencies and applied loads, and then the buckling load is calculated. In this method, the vibrational mode shape must be identical to buckling mode shape to provide high-precision results.

The VCT has been developed by many researchers for conventional structures such as columns, flat plates, and shells by Chu [21], Johnson and Goldhammer [22], Radhakrishnan [23], Chailleux [24], Jubb et al. [25], Singer and Abramovich [26] and Plaut and Virgin [27] in the last recent decades. A detailed state-of-the-art review on the VCT was carried out in chapter 15 of Ref. [28]. Singhatanadgid and Sukajit [29, 30] presented the VCT to calculate the buckling load of rectangular thin plates. When the applied load comes close to the buckling load of the plate, its natural frequency approaches zero. Actual boundary conditions and critical buckling load of unstiffened plates and cylindrical shells were estimated numerically and experimentally by Arbelo et al. [31]. It was shown that the VCT is capable to evaluate boundary conditions and then improving the buckling load. In another work, a proposed VCT approach in Ref. [31] was experimentally validated by Arbelo et al. [32] to predict the buckling load of unstiffened cylindrical shells. They showed that the proposed approach gives a suitable correlation when the maximum applied load is higher than 50% of the experimental buckling load. Using the VCT, the buckling load of stringer stiffened curved panels was calculated by Abramovich et al. [33]. Similar to Ref. [32], a reasonable correlation was obtained when the maximum applied load is higher than 50% of the experimental buckling load. The buckling behavior and the modal

analysis of the stiffened CFRP plate were numerically and experimentally investigated using the VCT by Chaves-Vargas et al. [34]. Skukis et al. [35] presented the experimental VCT to estimate the buckling load of the unstiffened cylindrical shells. It was shown that when the applied load is greater than 80% of the buckling load a good correlation is achieved. Shahgholian-Ghahfarokhi and Rahimi performed a experimental and numerical investigation of the VCT approach proposed in [31] to evaluate the buckling behavior of grid-stiffened composite cylindrical shells. It was shown that there is a good correlation between numerical and experimental approaches if nonlinear effects, such as geometric and thickness imperfection, were considered. Recently, Franzoni et al. [36] proposed experimental validation of the VCT defined in [31] to estimate the buckling load of unstiffened composite cylindrical shells. In another work, the buckling load of a pressurized orthotropic cylindrical shell was obtained using the mentioned VCT by Franzoni et al. [37]. It was shown that the approach proposed in [31] provided a better buckling load estimation for the tests associated with greater magnitudes of the knockdown factor, which is the ratio between the experimental buckling load and the critical buckling load. Furthermore, analytical and numerical validation of the afore-mentioned VCT were introduced by Franzoni et al. [38]. The authors illustrated the developed analytical support through a numerical study based on theoretical thin-walled unstiffened cylindrical shells. As observed in previous publications [32, 35-37], the methodology provided suitable results when the maximum applied load level is higher than 50% of the nonlinear buckling load. Shahgholian-Ghahfarokhi and et al. [39] presented the experimental and numerical validation of the VCT approach to estimate the buckling load of composite sandwich plates with iso-grid cores. The authors showed that there is a good accord between the buckling loads estimated through the VCT and the one obtained from the static test. . In addition, it was shown that a load level up to 67% experimental load is sufficient for reasonable estimations.

Although great attention has been paid on the buckling load prediction of conventional structures such as beams, simple plates, and shells, this technique is still under development for composite sandwich structures. Besides, analytical, numerical, and experimental VCT for CLSC has not been spotted in the literature, to the best of the authors' knowledge. Therefore, this article discusses the VCT for predicting the buckling load of CLSC through numerical and experimental studies. As well, an analytical formulation for the free vibration of axially loaded CLSC is presented. The analytical formulation is obtained employing the Rayleigh-Ritz method considering FSDT, yielding the dynamic behavior of an axially loaded CLSC and its critical buckling load. Afterward, three linear and nonlinear numerical analyses are considered. The critical buckling load and first natural frequency for different axially applied load levels are firstly calculated and compared to the analytical results for validation of the numerical models. Then, another FE model is defined considering geometric nonlinearities and initial imperfections for obtaining the variation of the first natural frequency with the axially applied load. As well, the nonlinear buckling analysis is also performed using the Riks method for a better comparison with the VCT results. Finally, four specimens are fabricated using a filament winding setup. Furthermore, a buckling test is carried out to validate the results of the VCT approach. Finally,

the obtained buckling load using the VCT is validated based on the buckling loads calculated from the nonlinear Riks method and measured during the static experimental campaign.

2. The considered CLSC geometry

In this paper, the CLSC geometry is considered as shown in Fig. 1. Composite lattice sandwich cylinders composed of an inner skin, an outer skin, and a lattice core, which is established from the many helical stiffeners. Figure 1 presents the main geometrical parameters, i.e., L as the length of CLSC, r as the average radius of CLSC, and t_o, t_i, and t_s as the thicknesses of the outer skin, inner skin, and stiffeners, respectively. Additionally, w is the stiffener's width. The considered geometrical parameters are given in Table 1.

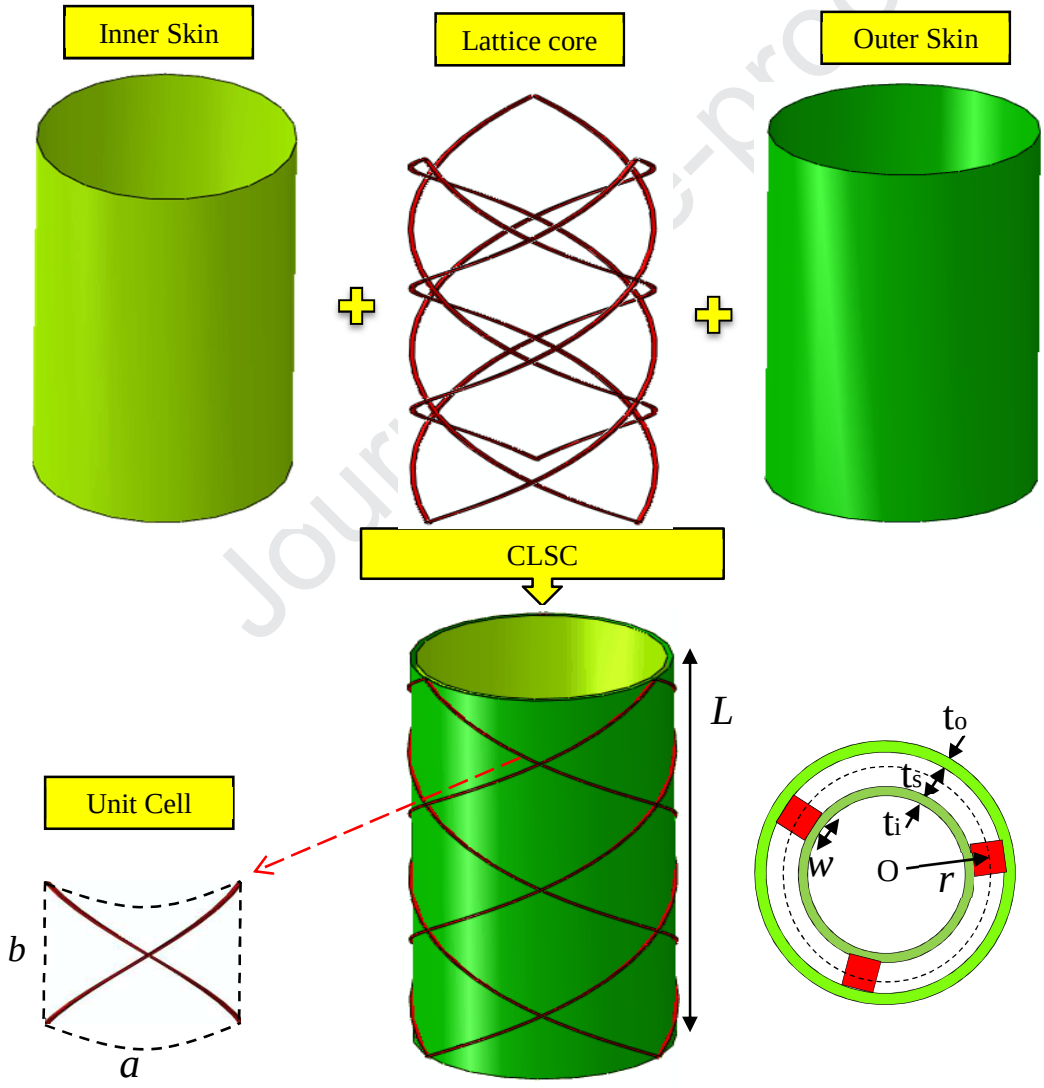

Fig. 1. The CLSC geometry.

Table 1 The considered geometrical parameters.

Parameter	Value
L (mm)	300
r (mm)	80
t_o (mm)	1.25
t_i (mm)	1.25
t_s (mm)	3
w (mm)	4
N_a	3
N_C	3

It should be noted that the lattice core consists of many unit cells. The unit cell is selected in such a way that the whole lattice core can be generated by the repetition of this unit cell. In the analytical section, which is explained in section 4, the equivalent stiffness parameters of this unit cell are obtained and then utilized to the whole lattice core. This is valid as the whole lattice core can be reproduced from this unit cell. As shown in Fig. 1, a and b are defined as the width and length of the unit cell respectively. The a is calculated by $a = \frac{2\pi r}{N_c}$, where N_c is the number of unit cells in the circumferential direction. Also, the b is calculated by $= \frac{L}{N_a}$, where N_a is the number of unit cells in the axial direction.

3. The VCT implementation procedure

The general steps to implement the VCT on CLSC are listed below [38, 39]:

1. The natural frequency at zero load ω_{mn} and the critical buckling load P_{cr} of the perfect structure are calculated. In this paper, ω_{mn} and P_{cr} are obtained using both analytical and numerical methods.
2. The natural frequency variation during axial loading is obtained. In this paper, the present step is carried out using nonlinear finite element results.
3. The square of the drop of the load-carrying capacity due to initial imperfections ξ^2 is obtained from the appropriate characteristic chart. By tracking the open literature, two general approaches are available to calculate ξ^2 for imperfection-sensitive structures, as given below.

A) First approach:

A linear relationship between the $(1-p)^2$ and the $(1-f^4)$ was proposed by Souza et al. [40, 41]:

$$(1-p)^2 + (1-\xi^2)(1-f^4) = 1 \quad (1)$$

where $f = \frac{\bar{\omega}_{mn}}{\omega_{mn}}$ and $p = \frac{P_a}{P_{cr}}$, being P_a the the applied axial load, $\bar{\omega}_{mn}$ the measured frequency at P_a. Besides, m is the number of axial half-waves and n is the number of circumferential waves (for CLSC).

The drop of the load-carrying capacity due to initial imperfections is defined as the value of $(1-p)^2$ related to $(1-f^4)$ equaling to one from the linear best-fit between $(1-p)^2$ versus $(1-f^4)$, as illustrated in Fig. 2a.

B) The Second approach:

According to the limitation of the first VCT pointed out in [31], a modified methodology has been introduced in the quoted paper. They proposed a second-order curve fitting between $(1-p)^2$ versus $(1-f^2)$ as shown in Fig. 2b. In this approach, ξ^2 is defined as the minimum value of $(1-p)^2$ from graph $(1-p)^2$ versus $(1-f^2)$. Until now, this approach has been validated for unstiffened plate and shell [32, 36], with and without cutouts [42], grid-stiffened shell [43], variable angle tow shell [44], lattice sandwich plate [39], pressurized orthotropic shell [37].

Thus, this paper will consider the presented VCTs, investigating their applicability for CLSC.

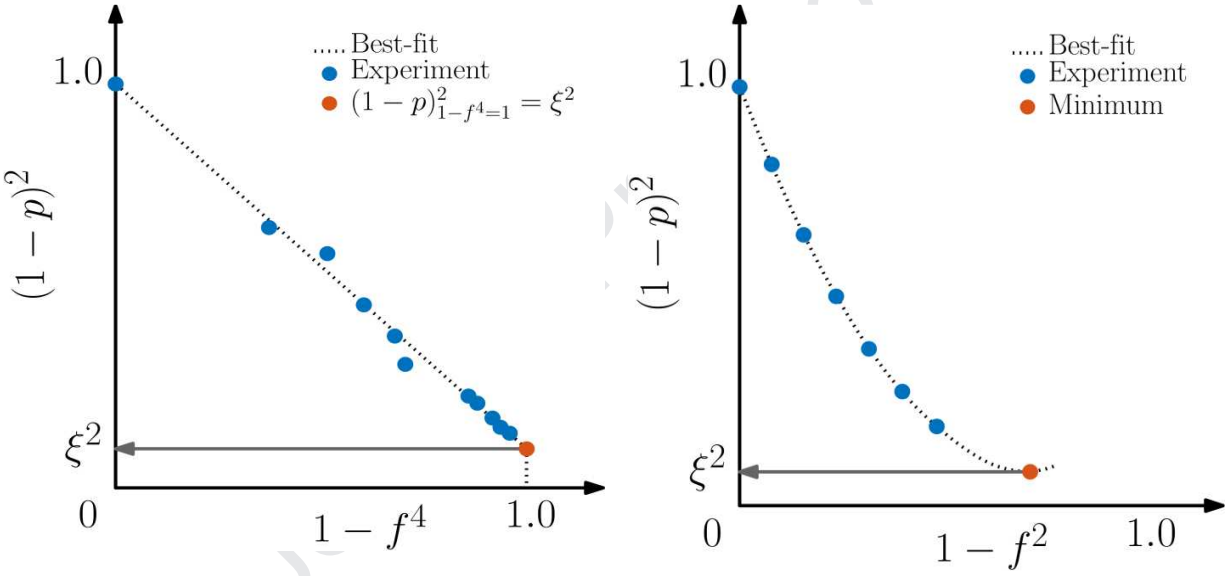

(a) First VCT approach [36, 38, 40] (b) Second VCT approach [31, 32]

Fig. 2. Schematic view of different VCT approach.

4. In the final step, the buckling load of shell is estimated through the VCT as proposed in [31, 32, 36-39, 42, 43, 45].

$$P_{VCT} = P_{cr}(1-\sqrt{\xi^2}) \tag{2}$$

where P_{CR} is the critical buckling load of the perfect structure and P_{VCT} is the estimated buckling load for imperfect structure.

4. Analytical VCT approach for perfect CLSC

As revisited in the literature review, the VCT has been widely used for predicting the buckling load of structures such as beam, plate, and unstiffened shells. Nevertheless, only a few studies have addressed the analytical aspects of the VCT, being most of these studies developed for the conventional structures listed above. For example, Franzoni et al. [38] provided analytical support for the methodology proposed in [31]. The authors established this support for an unstiffened cylinder employing the linearized Flügge-Lur'e-Byrne's theory of shells. According to this explanation, the analytical formulation for CLSC has significant innovations. Consequently, this section presents the free vibration of an axially loaded CLSC. In a similar approach to the buckling problem of CLSC, which presented by the authors in the Ref. [18], the free vibration analysis of an axially loaded perfect CLSC is carried out in the present paper. This study allows verifying the numerical results that have been used for calculating the buckling load of CLSC.

4.1. *Displacement and strain fields of CLSC*

This paper utilizes FSDT with the following displacement field obtained from Ref. [17, 18]:

$$\begin{aligned} u(\theta,x,t) &= u_0(\theta,x,t) + (\tfrac{t_o-t_i}{4})\varphi_x \\ v(\theta,x,t) &= v_0(\theta,x,t) + (\tfrac{t_o-t_i}{4})\varphi_\theta \\ w(\theta,x,t) &= w_0(\theta,x,t) \end{aligned} \tag{3}$$

where *u*, *v*, and *w* represent the displacements along x-, y-, and z-axes; u_0, v_0, and w_0 are mid-plane displacements in longitudinal, circumferential, and radial directions; φ_x and φ_θ are the rotation of the middle plane with respect to the neutral surface of the CLSC in θ and *x*-direction; and t denotes the time.

According to general strain–displacement relationships for cylindrical shells, mid-plane strains, curvatures, and shear strain of the CLSC are considered by $\varepsilon = [\varepsilon_x^0, \varepsilon_\theta^0, \gamma_{x\theta}^0]$, $\kappa = [\kappa_x, \kappa_\theta, \kappa_{x\theta}]$, and $\gamma = [\gamma_{xz}, \gamma_{\theta z}]$, respectively, which are given by [46].

$$\begin{aligned} \varepsilon_x^0 &= \frac{\partial u_0}{\partial x} \\ \varepsilon_\theta^0 &= \frac{1}{r}\frac{\partial v_0}{\partial \theta} + \frac{w_0}{r} \\ \gamma_{x\theta}^0 &= \frac{\partial v_0}{\partial x} + \frac{1}{r}\frac{\partial u_0}{\partial \theta} \\ \kappa_x &= \frac{\partial \varphi_x}{\partial x} \\ \kappa_\theta &= \frac{1}{r}\frac{\partial \varphi_\theta}{\partial \theta} \\ \kappa_{x\theta} &= -\frac{1}{r}\frac{\partial \varphi_x}{\partial \theta} + \frac{\partial \varphi_\theta}{\partial x} \\ \gamma_{xz} &= \frac{\partial w_0}{\partial x} + \varphi_x \\ \gamma_{\theta z} &= \frac{1}{r}\left(\frac{\partial w_0}{\partial \theta} - v_0\right) + \varphi_\theta \end{aligned} \tag{4}$$

4.2. *Total stiffness of CLSC*

The total stiffness of CLSC is calculated from the combination of the inner skin, outer skin, and stiffeners' stiffness. By using the superposition method, which is explained in Ref. [47, 48], the total stiffness of CLSC is obtained:

$$[S] = [S]^{\text{outer skin}} + [S]^{\text{st}} + [S]^{\text{inner skin}} \tag{5}$$

where $[S]^{\text{outer skin}}$, $[S]^{\text{inner skin}}$, and $[S]^{\text{st}}$ are stiffness of the outer skin, inner skin, and stiffeners, respectively.

4.2.1. Outer/inner skin stiffness

The skin stiffness is obtained as Eq. (6) [18].

$$[S]^{\text{skin}} = \begin{bmatrix} [A]^{\text{skin}} & [B]^{\text{skin}} & 0 \\ [B]^{\text{skin}} & [D]^{\text{skin}} & 0 \\ 0 & 0 & [A_s]^{\text{skin}} \end{bmatrix} \tag{6}$$

Where A^{skin}, B^{skin}, D^{skin}, and ${A_s}^{\text{skin}}$ are the stiffness parameters of skin, which corresponds to the extensional, coupling, bending, and shear matrices, respectively.

The above components can be calculated based on the lamination theory [49]:

$$[{A_{ij}}^{\text{skin}}] = \sum_{k=1}^{n} [\overline{Q}_{ij}{}^{k}](z_{(k+1)} - z_k) \qquad (i,j = 1,2,6) \tag{7}$$

$$[{B_{ij}}^{\text{skin}}] = \frac{1}{2}\sum_{k=1}^{n} [\bar{Q}_{ij}{}^{k}]({z^2}_{(k+1)} - {z^2}_{k}) \qquad (i,j = 1,2,6) \tag{8}$$

$$[{D_{ij}}^{\text{skin}}] = \frac{1}{3}\sum_{k=1}^{n} [\bar{Q}_{ij}{}^{k}]({z^3}_{(k+1)} - {z^3}_{k}) \qquad (i,j = 1,2,6) \tag{9}$$

$$[{A_s}^{\text{skin}}] = \frac{5}{4}\sum_{k=1}^{n} [\bar{Q}_{ij}{}^{k}]\left(z_{(k+1)} - z_k - \frac{4}{3t^2}({z^3}_{(k+1)} - {z^3}_{k})\right) \qquad (i,j = 4,5 \text{ only}) \tag{10}$$

where $[\overline{Q}_{ij}{}^{k}]$ are the transformation reduced plane stiffness matrix, for $i,j = 1,2,6$, and $[\overline{Q}_{ij}]$ are the transformation transverse shear stiffness matrix, for $(i,j = 4,5)$.

In Eq. (10), it is assumed that the transverse shear stresses are distributed parabolically across the laminate thickness [49]. In spite of discontinuities at the interface between lamina, a continuous function $f(z) = \frac{5}{4}[1 - \left(\frac{2z}{h}\right)^2]$ is used as a weighting function by some authors, which includes a factor of 5/4 so that the shear factor calculated for layer orthotropic shell wall is consistent with the established shear factor from the previous work for the homogeneous case.

4.2.2. The stiffness of stiffeners

Similar to Eq. (6), the stiffness of stiffeners is obtained as presented in Eq. (11).

$$[S]^{\mathrm{st}} = \begin{bmatrix} [A]^{\mathrm{st}} & [B]^{\mathrm{st}} & 0 \\ [B]^{\mathrm{st}} & [D]^{\mathrm{st}} & 0 \\ 0 & 0 & [A_s]^{\mathrm{st}} \end{bmatrix} \tag{11}$$

Where A^{st}, B^{st}, D^{st}, and ${A_s}^{st}$ are the stiffness parameters of stiffeners, which correspond to the extensional, coupling, bending, and shear matrices, respectively. These matrices are calculated as [18]:

$$[A]^{st} = 2A \begin{bmatrix} \frac{E_l c^3 - 2G_{lt} cs^2}{a} & \frac{E_l cs^2 + 2G_{lt} cs^2}{a} & 0 \\ \frac{E_l sc^2 + 2G_{lt} sc^2}{b} & \frac{E_l s^3 - 2G_{lt} sc^2}{b} & 0 \\ 0 & 0 & \frac{E_l sc^2 + G_{lt} sc^2 - G_{lt} s^3}{b} \end{bmatrix} \tag{12}$$

$$[B]^{st} = \frac{A(t_o - t_i)}{2} \begin{bmatrix} \frac{E_l c^3 - 2G_{lt} cs^2}{a} & \frac{E_l cs^2 + 2G_{lt} cs^2}{a} & 0 \\ \frac{E_l sc^2 + 2G_{lt} sc^2}{b} & \frac{E_l s^3 - 2G_{lt} sc^2}{b} & 0 \\ 0 & 0 & \frac{E_l sc^2 + G_{lt} sc^2 - G_{lt} s^3}{b} \end{bmatrix} \tag{13}$$

$$[D]^{st} = \frac{A(t_o - t_i)^2}{8} \begin{bmatrix} \frac{E_l c^3 - 2G_{lt} cs^2}{a} & \frac{E_l cs^2 + 2G_{lt} cs^2}{a} & 0 \\ \frac{E_l sc^2 + 2G_{lt} sc^2}{b} & \frac{E_l s^3 - 2G_{lt} sc^2}{b} & 0 \\ 0 & 0 & \frac{E_l sc^2 + G_{lt} sc^2 - G_{lt} s^3}{b} \end{bmatrix} \tag{14}$$

$$[A_s]^{st} = 2A \begin{bmatrix} \frac{G_{lz} c}{b} & 0 \\ 0 & \frac{G_{lz} s}{a} \end{bmatrix} \tag{15}$$

where $\mathrm{c} = \cos(\phi)$, $\mathrm{s} = \sin(\phi)$, and ϕ is the stiffener orientation angle with respect to the axial direction. Moreover, E_l, G_{lt}, and G_{lz} are longitudinal, shear in-plane l-t, and shear in-plane l-z moduli of the stiffeners, respectively. As well, A is the cross-sectional area of the stiffeners. According to Eq. (6) and (11), the stiffness parameters of the CLSC can be considered as:

$$[A] = [A]^{\text{outer skin}} + [A]^{st} + [A]^{\text{inner skin}} \tag{16}$$

$$[B] = [B]^{\text{outer skin}} + [B]^{st} + [B]^{\text{inner skin}} \tag{17}$$

$$[D] = [D]^{\text{outer skin}} + [D]^{st} + [D]^{\text{inner skin}} \tag{18}$$

$$[A_s] = [A_s]^{\text{outer skin}} + [A_s]^{\text{st}} + [A_s]^{\text{inner skin}} \tag{19}$$

4.3. *Energy Method*

To obtain natural frequencies at the different load levels and the buckling load, the Rayleigh-Ritz energy method is applied. According to this method, total strain energy U, the work W done by the external force, and kinetic energy K of the CLSC must be calculated in the first step.

The total strain energy U of the CLSC by FSDT can be derived as [46, 49]

$$U = \frac{1}{2}\int_0^{2\pi}\int_0^{L}(\varepsilon.[A].\varepsilon^T + \kappa.[D].\kappa^T + 2\varepsilon.[B].\kappa^T + \gamma.[A_s].\gamma^T)rdxd\theta \tag{20}$$

The potential energy due to the axial external force $\bar{P}$ is shown as follows:

$$W = -\frac{1}{2}\int_0^{2\pi}\int_0^{L}\frac{\bar{P}}{(2\pi r)}(\frac{\partial w}{\partial x})^2\, r\mathrm{d}x\mathrm{d}\theta \tag{21}$$

It should be noted that $\bar{P}$ is considered as the buckling load in the buckling analysis while it is considered as applied load in the free vibration of axially loaded CLSC.

The kinetic energy of the CLSC can be obtained as:

$$K = \frac{1}{2}\int_0^{2\pi}\int_0^{L}\int_{-\frac{t}{2}}^{\frac{t}{2}}\rho(z)[\left(\frac{\partial u}{\partial t}\right)^2 + \left(\frac{\partial v}{\partial t}\right)^2 + \left(\frac{\partial w}{\partial t}\right)^2]\, r\mathrm{d}z\mathrm{d}x\mathrm{d}\theta \tag{22}$$

where $\rho(z)$ is the density of the CLSC.

4.3.1. *Application of Ritz method and solution procedure*

In this section, two analyses are considered to obtain the natural frequencies at a different load level and the buckling load. Therefore, the total energy function $\prod$ is calculated by the sum of strain energy and potential energy due to the axial external force for the buckling analysis, while the sum of strain energy, kinetic energy, and potential energy due to the axial external force for the free vibration of an axially loaded CLSC. Hence, the following total energy function is considered for both buckling and vibration analyses [50, 51].

$$\prod = \begin{cases} U + W & \text{For the buckling analysis} \\ U + W - K & \text{For the free vibration of axially loaded analysis} \end{cases} \tag{23}$$

According to the Ritz method, admissible functions for the general displacement components should be considered to satisfy the boundary conditions and solve the buckling and vibration analyses. Consequently, Eq. (24) for the buckling analysis and Eq. (25) for the free vibration analysis can be assumed by considering the CLSC with two simply supported SS3 edges [38].

$$
\begin{aligned}
u_0 &= \sum_{m=1}^{\infty}\sum_{n=1}^{\infty} A_{mn}\cos\left(\frac{m\pi}{L}x\right)\cos(n\theta)\\
v_0 &= \sum_{m=1}^{\infty}\sum_{n=1}^{\infty} B_{mn}\sin\left(\frac{m\pi}{L}x\right)\sin(n\theta)\\
w_0 &= \sum_{m=1}^{\infty}\sum_{n=1}^{\infty} C_{mn}\sin\left(\frac{m\pi}{L}x\right)\cos(n\theta)\\
\varphi_x &= \sum_{m=1}^{\infty}\sum_{n=1}^{\infty} D_{mn}\cos\left(\frac{m\pi}{L}x\right)\cos(n\theta)\\
\varphi_\theta &= \sum_{m=1}^{\infty}\sum_{n=1}^{\infty} E_{mn}\sin\left(\frac{m\pi}{L}x\right)\sin(n\theta)
\end{aligned}
\tag{24}
$$

$$
\begin{aligned}
u_0 &= \sum_{m=1}^{\infty}\sum_{n=1}^{\infty} A_{mn}\cos\left(\frac{m\pi}{L}x\right)\cos(n\theta)\cos(\omega_{mn}t)\\
v_0 &= \sum_{m=1}^{\infty}\sum_{n=1}^{\infty} B_{mn}\sin\left(\frac{m\pi}{L}x\right)\sin(n\theta)\cos(\omega_{mn}t)\\
w_0 &= \sum_{m=1}^{\infty}\sum_{n=1}^{\infty} C_{mn}\sin\left(\frac{m\pi}{L}x\right)\cos(n\theta)\cos(\omega_{mn}t)\\
\varphi_x &= \sum_{m=1}^{\infty}\sum_{n=1}^{\infty} D_{mn}\cos\left(\frac{m\pi}{L}x\right)\cos(n\theta)\cos(\omega_{mn}t)\\
\varphi_\theta &= \sum_{m=1}^{\infty}\sum_{n=1}^{\infty} E_{mn}\sin\left(\frac{m\pi}{L}x\right)\sin(n\theta)\cos(\omega_{mn}t)
\end{aligned}
\tag{25}
$$

where A_{mn}, B_{mn}, C_{mn}, D_{mn}, and E_{mn} are the amplitude coefficients. For the stable equilibrium, the total potential energy shall be at the minimum. This can be satisfied by finding the first derivative of the total potential energy $\prod$ with respect to the unknown constants A_{mn}, B_{mn}, C_{mn}, D_{mn} and E_{mn} equating to zero as below:

$$\frac{\partial \prod}{\partial A_{mn}} = 0 \tag{26}$$

$$\frac{\partial \prod}{\partial B_{mn}} = 0 \tag{27}$$

$$\frac{\partial \prod}{\partial C_{mn}} = 0 \qquad \text{Where } \begin{pmatrix} m = 1,2,\dots,i \\ n = 1,2,\dots,j \end{pmatrix} \tag{28}$$

$$\frac{\partial \prod}{\partial D_{mn}} = 0 \tag{29}$$

$$\frac{\partial \prod}{\partial E_{mn}} = 0 \tag{30}$$

This process results in Eq. (31) for the buckling analysis and Eq. (32) for the vibration analysis:

$$\left([\mathrm{K}_e] - \bar{P}[\mathrm{K}_g]\right)\Delta = 0 \quad \text{where } (\Delta)^{\mathrm{T}} = (A, B, C, D, E) \tag{31}$$

$$([\mathrm{K}_e] - \omega^2[\mathrm{M}])\Delta = 0 \quad \text{where } (\Delta)^{\mathrm{T}} = (A, B, C, D, E) \tag{32}$$

where $[\mathrm{K}_e]$, $[\mathrm{K}_g]$, and $[\mathrm{M}]$ are the stiffness, geometric, and mass matrices, respectively. Searching for the stability limit one derives Eq. (31), which is formally equivalent to Eq. (32), both providing generic eigenvalue problems with the critical buckling loads and natural frequency as the lowest eigenvalues. A MATLAB code was written to obtain the critical buckling load and natural frequency satisfying this condition. In this code, the maxima of both m and n are 100, so 10000 coefficients are calculated for sample analysis.

5. Finite element analyses

In this section, finite element analyses are carried out to calculate linear buckling load, linear natural frequency, natural frequencies at the different load levels, and the nonlinear buckling load. For this purpose, ABAQUS CAE software is selected. The outer and inner skins are created by extruding a circle with radii of 81.5 and 78.5 mm, respectively. Moreover, the outer and inner skins are established as a laminate considering the eight-layered lay-up $[0, 90]_8$. In a similar manner, stiffeners are modeled as 3D bulks by considering a proper height and square cross-section area. The composite lay-up module is used to assign the material properties to skins and stiffeners. The so-called TIE constraints are also used to stick the stiffeners to outer and inner skins. The outer and inner skins and stiffeners have been meshed using the quadratic planar elements with 8 nodes S8R and brick elements with reduced integration with 20 nodes C3D20R, respectively. Convergence analyses were performed, providing the number and size of elements. According to the mentioned analyses, the optimal size of the element was defined as approximately 3.2 mm. Consequently, the total number of S8R and C3D20R elements were 34930 and 5008, respectively. The final model is presented in Fig. 3. As can be seen, two epoxy tabs with 15 mm height are fabricated at the top and bottom edges of the CLSC structure for suitable load distribution in the experimental test. By considering the mentioned tabs, all of the displacements and rotations are zero for the CLSC edges. It should be noted that the axial displacement of the top edge of the CLSC u is not zero for the buckling analysis and applying the axial load. According to this explanation, the clamp-clamp (C-C) boundary conditions are the most appropriate boundary conditions that describe the real conditions.

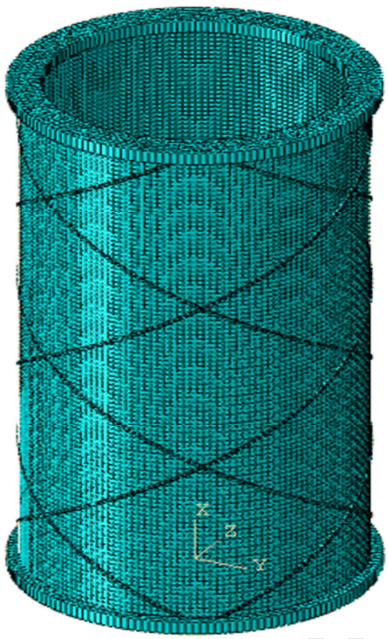

Fig. 3. Final FE model.

After making the final model, which has been explained above, three main analyses were defined, which are as described in the next subsections.

5.1. *Linear buckling and free vibration analyses of the perfect CLSC*

The linear buckling and free vibration analyses are performed to obtain the critical buckling load P_{cr} and the natural frequency at the zero load level ω_{mn}, which are used for the VCT predictions and a comparison with the analytical results. In two linear analyses, the nominal geometry is considered without initial geometric imperfection. The default Lanczos solver was employed for the linear buckling and free vibration analyses.

5.2. *Nonlinear free vibration of axially loaded CLSC analysis*

In this analysis, the geometrical imperfections are accounted for in the FE model. The general steps for the implementation of this analysis are itemized below.

-Step 1: The geometric imperfections shall be measured. For this purpose, there are several methods [31, 32, 52]. In this paper, the CLSC is divided with 10 and 12 grid points in the axial and circumferential directions. Then, the radial imperfections are measured at these grid points. The geometric imperfection results are shown in Fig. 4.

-Step 2: The measured geometric imperfection is imported into the FE model through shifting the radial position of each node, using an inverse weighted interpolation rule with the five closest measured points from the imperfection data file. This method is fully explained in Ref. [52].

-Step 3: The axial compressive loads are applied on the CLSC up to the desired magnitude. For this purpose, the Newton-Raphson algorithm with artificial damping stabilization can be used as a nonlinear solver.

-Step 4: Once an applied load is reached, the vibration analysis is performed to calculate the natural frequencies of the CLSC.

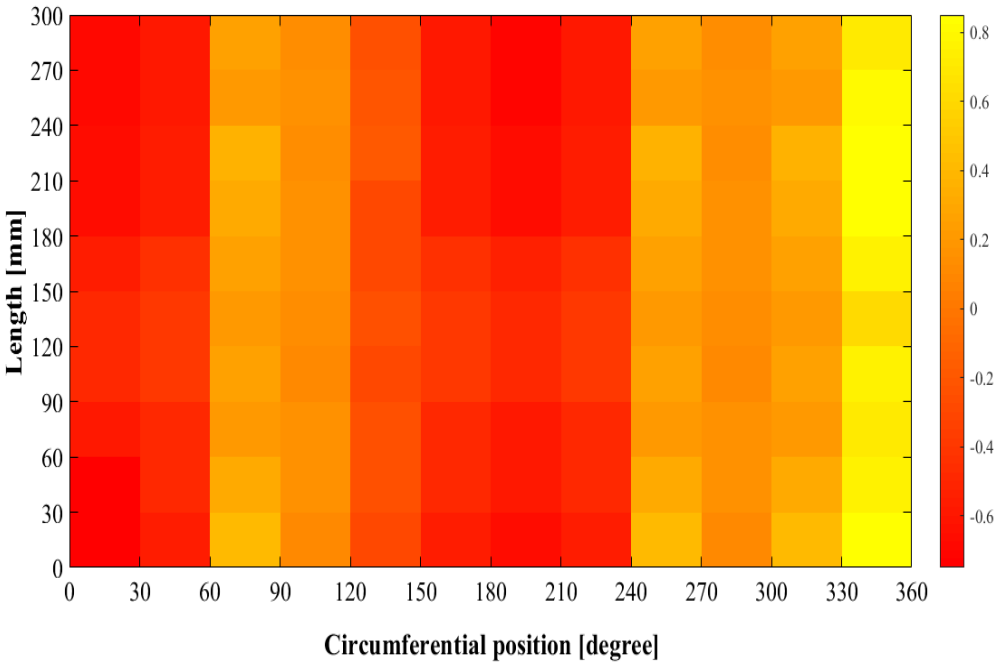

Fig. 4. Geometric imperfection results.

For a better comparison of the VCT results, the nonlinear buckling analysis is also performed using the static Riks method. Within this model, the initial imperfections are implemented by multiplying the eigenmodes obtained from a linear analysis by a scaling factor.
In this study, the first linear buckling mode, as suggested in [53], was used for disturbing the FE mesh. Moreover, the scaling factor was assumed as the maximum deviation measured in step 1 described in Subsection 5.2, i.e., 0.85 mm. This method is described in detail in Refs. [39, 43, 52].

6. Fabrication and experimental buckling test

6.1. *Material properties*

In this research, the outer and inner skins were fabricated from glass woven fabric with density 200 gr/m^2 and room-temperature-curing epoxy matrix. Besides, E-glass fibers with a density of 2.4 kg/m^3 and room-temperature-curing epoxy matrix were used to make the stiffeners as well as the lattice core. As per to ASTM D-2584, ASTM D3039M, ASTM D3410, and ASTM-D3518 standards, the mechanical material properties of fibers, resin, as well as outer/inner skin, were obtained. These results are given in Table 2. In addition, the mechanical material properties of the stiffeners were calculated using a micromechanical approach [54], which is also reported in Table 2.

Table 2 Mechanical material properties of the skin and stiffeners.

Property		Outer and inner Skins	Stiffeners
Density (kg/m^3)	ρ	1537	1152
Young's Modulus (GPa)	E_1	6.43	10.91
	E_2	6.43	1.273
	E_3	-	1.273
Shear Modulus (GPa)	$G_{12} = G_{13}$	0.96	0.457
	G_{23}	1.12	0.565
Poisson's ratio	$\vartheta_{12} = \vartheta_{13}$	0.28	0.304
	ϑ_{23}	0.087	0.127

6.2. *CLSC fabrication method*

To fabricate the lattice sandwich structures, several methods are available; [7, 8, 39, 43, 55]. In this paper, the method that has been explained in detail in Ref. [43], was applied to fabricate the CLSC. For this purpose, the silicone rubber mold is firstly designed and fabricated using a polexi glass tool. Subsequently, it was installed onto the polyethylene mandrel for winding as shown in Fig. 5. Using a filament winding machine, the stiffeners, as well as, lattice core, were fabricated as shown in Fig. 6a. After this, a layer of fabric was placed on the stiffeners and mixed with resin. This work continues until the total number of layers is reached. Therefore, the grid-stiffened cylinder, which consists of the outer skin and lattice core, was fabricated as shown in Fig. 6b. Using a similar way used for the outer skin, the inner skin was fabricated separately as shown in Fig. 6c. Finally, the inner skin was placed inside the grid-stiffened cylinder and was attached to the inner surface of the lattice core. To prevent the local buckling and suitable force distribution at the top and bottom edges, two epoxy rings were fabricated and placed at the top and bottom edges of the CLSC. As shown in Fig. 7, four identical CLSC were fabricated which were designated as T1, T2, T3, and T4.

6.3. *Experimental buckling test*

The numerical results of the VCT must be confirmed by the experimental ones. For this purpose, buckling experiments were performed and the corresponding experimental buckling loads P_{EXP} obtained. As shown in Fig. 8, the universal compressive testing machine was used to perform the buckling test on the CLSC. The fabricated specimens were tested up to the buckling load P_{EXP} with a loading rate of 2 mm/min. It should be mentioned that the buckling test was repeated four times to increasing its accuracy and reliability. Figure 9 presents the load-displacement curves for four specimens. Besides, the obtained results are presented in Table 3.

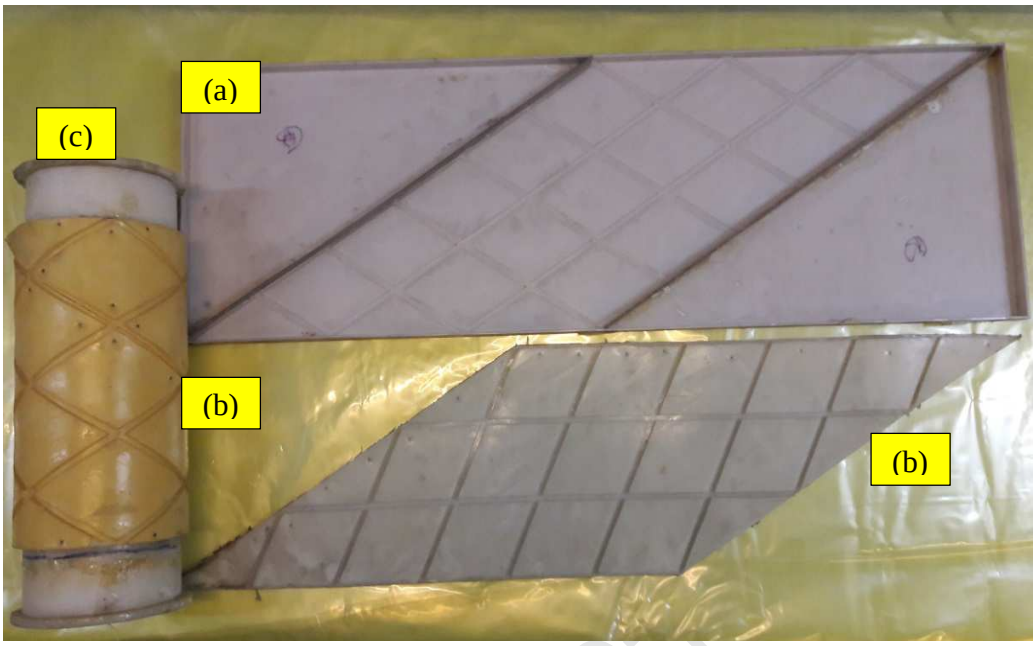

Fig. 5. Fabrication tools, (a) Polexi glass tool, (b) Silicone rubber mold (c) polyethylene mandrel.

(a) Filament winding process (b) Grid stiffened cylinder (c) Inner skin

Fig. 6. Manufacturing process.

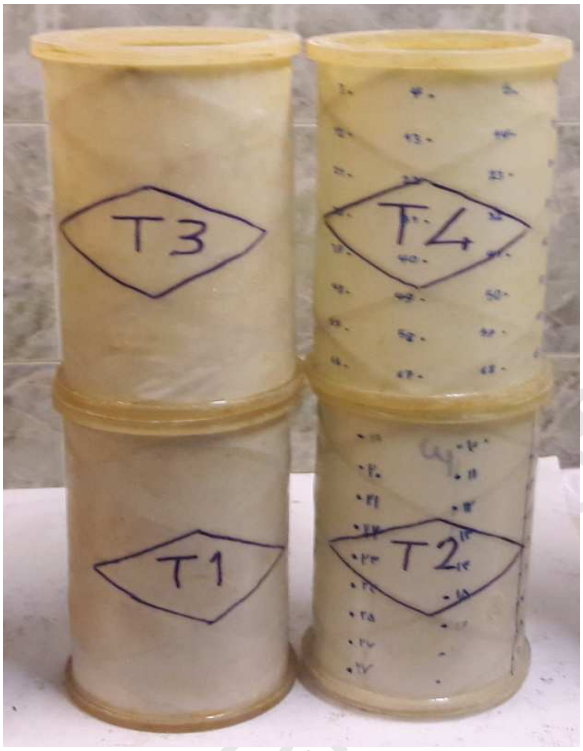

Fig. 7. The manufactured CLSC.

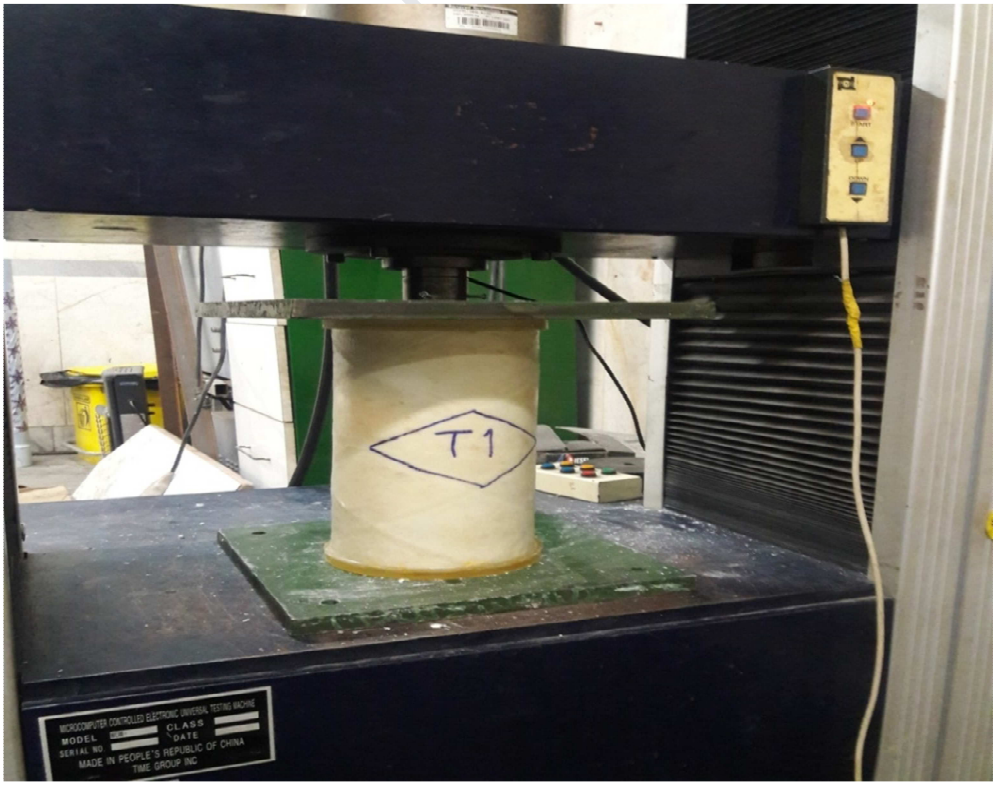

Fig. 8. Experimental buckling test.

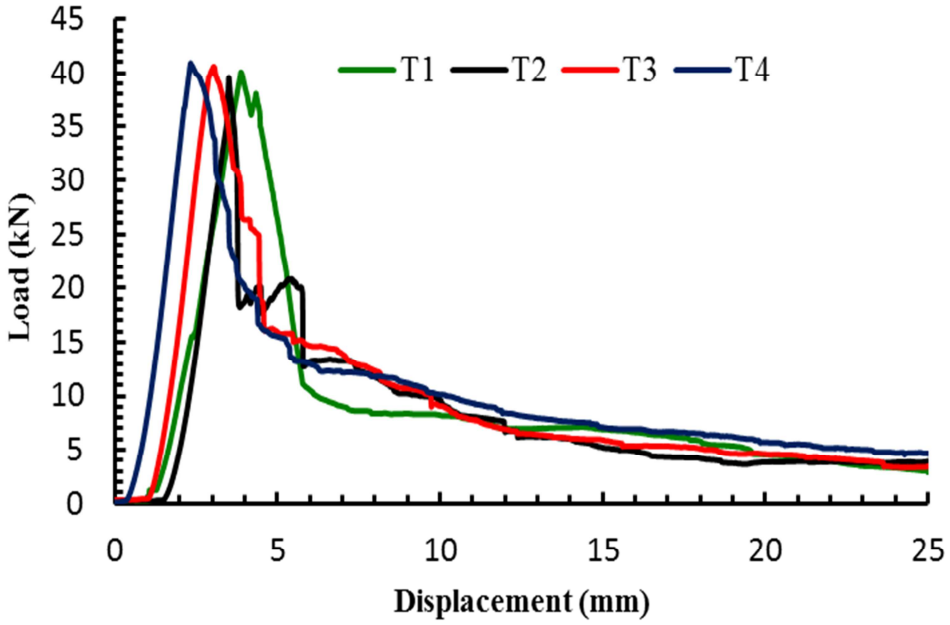

Fig. 9. The load-displacement curves for four specimens.

Table 3 Experimental buckling load of four fabricated CLSC.

Specimen number	Experimental buckling load (P_{EXP}) [kN]
T1	40.10
T2	39.75
T3	40.50
T4	40.72
Average	40.27

7. Results

7.1. *Analytical and numerical results of the perfect CLSC*

The analytical and numerical results for the linear buckling load and the first natural frequency at different load levels of the perfect CLSC are presented in Table 4. The analytical buckling load and natural frequencies were obtained from Eqs. (31) and (32), respectively. From Table 4, it is clear that the analytical and numerical results are in good agreement, and the maximum difference between them is less than 1.1%. Besides, Fig. 10 presents the first unloaded vibration and first buckling modes for perfect CLSC considering SS3 boundary conditions. From this figure, it can be noticed that the first unloaded vibration mode and the first buckling mode exactly match, which is expected for SS3 boundary conditions [38, 56]. It should be noted that the buckling and vibration modes were associated with the pairs (m, n): (1, 3).

From the above results, it can be concluded that the analytical approach has a high accuracy to predict the behavior of loaded CLSC. This method can be developed for imperfection-sensitive CLSC in future works.

Table 4 Analytical and numerical results of the perfect CLSC.

Variable	Analytical	FEM	$\delta = \frac{\lvert\text{Analytical} - \text{FEM}\rvert}{\text{FEM}} \times 100$
P_{cr} [kN]	50.46 (1, 3)	50.11 (1, 3)	0.70%
ω_{mn} [Hz]	489.24 (1, 3)	490.95 (1, 3)	0.35%
$\bar{\omega}_{mn}$ [Hz] at 25% of P_{cr}	463.12 (1,3)	464.60 (1,3)	0.32%
$\bar{\omega}_{mn}$ [Hz] at 50% of P_{cr}	431.84 (1, 3)	433.54 (1, 3)	0.39%
$\bar{\omega}_{mn}$ [Hz] at 75% of P_{cr}	396.26	393.18 (1,3)	0.78%
$\bar{\omega}_{mn}$ [Hz] at 90% of P_{cr}	362.10 (1, 3)	358.21 (1, 3)	1.08%

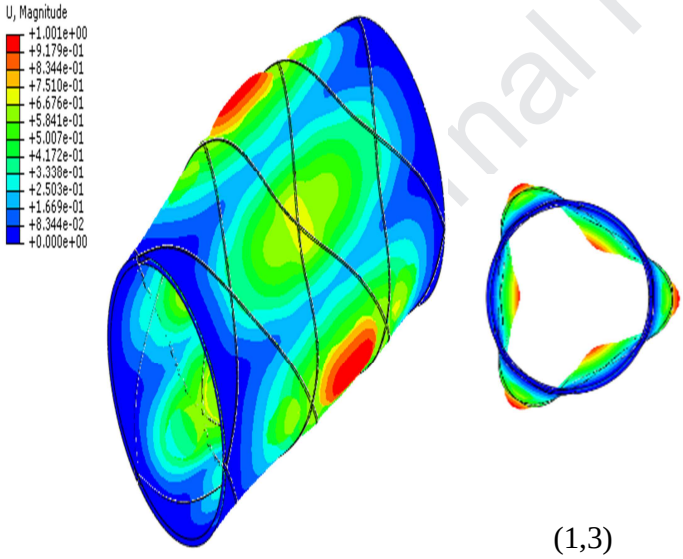

(a) First buckling mode

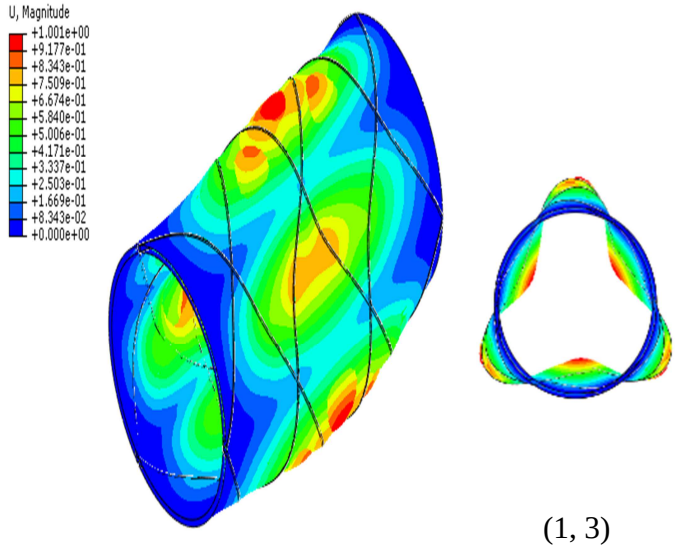

(a) First unloaded vibration mode

Fig. 10. First buckling and vibration modes of CLSC.

7.2. *Results of VCT approach for imperfection-sensitive CLSC*

Firstly, the linear buckling load and the first natural frequency were obtained considering (C-C) boundary conditions similar to the previous section. The linear buckling load and first natural frequency are 51.2 kN and 523.39 Hz, respectively. After this, the vibration analyses were

performed for imperfection-sensitive CLSC from zero load until 40 kN with a 5 kN increment. The natural frequencies at different levels of axially applied load are given in Table 5.

Table 5 Variations of the first vibration frequency with the applied load.

Axial compressive load (kN)	1st Natural frequencies [Hz]
0	523.39
5	513.32
10	502.70
15	491.44
20	479.38
25	466.34
30	455.26
35	443.81
40	419.37

The ξ^2 is calculated based on the two VCT approaches described in Section 3.

7.2.1. *Results of the first VCT approach*

For the first VCT approach, ξ^2 was calculated based on a linear best-fit equation obtained in the characteristic chart $(1-p)^2$ versus $(1-f^4)$, as shown in Fig. 11. As can be seen, this procedure resulted in a negative value for ξ^2, which does not have a physical meaning. Consequently, the VCT approach proposed by Souza et al. [40, 41] is unable to estimate the buckling load of CLSC, being not suitable for CLSC structures. It should be noted that similar results were presented in [31], where the authors have shown that this VCT approach is not suitable for estimating the buckling load of unstiffened composite cylindrical shells.

7.2.2. *Results of second VCT approach*

According to the second VCT approach introduced by Arbelo et al. [31, 32], ξ^2 is obtained from the characteristic chart $(1-p)^2$ versus $(1-f^2)$, as shown in Fig. 12. The second-order equation, ξ^2 is calculated as the minimum of such an equation.The magnitude of ξ^2 and the predicted buckling load using the VCT P_{VCT} are presented in Table 6. According to Table 6, the buckling load of the CLSC structure was estimated as 41.22 kN, considering a maximum applied load level of 78.1% of the linear buckling load P_{cr}.

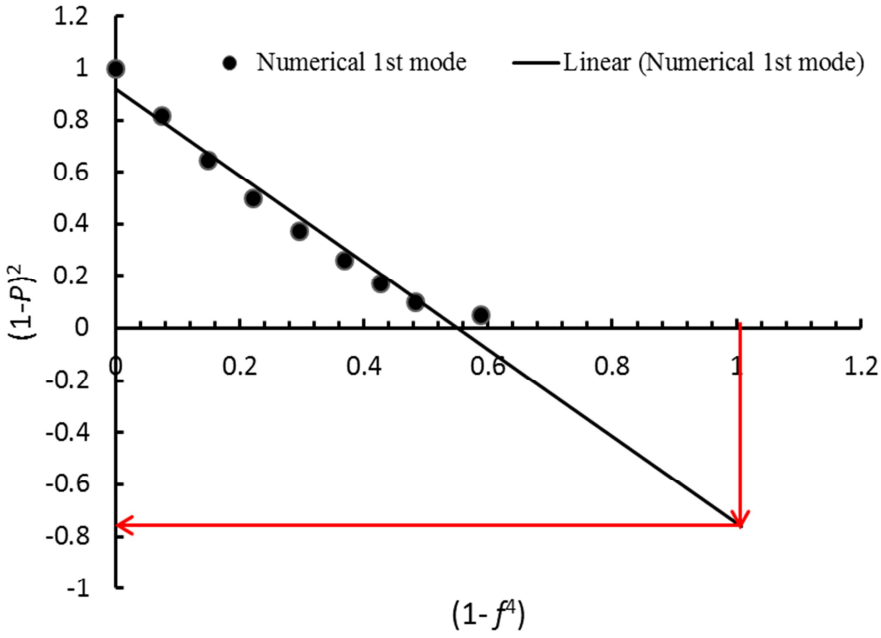

Fig. 11. First VCT approach (Proposed by Souza et al. [40, 41]) for CLSC.

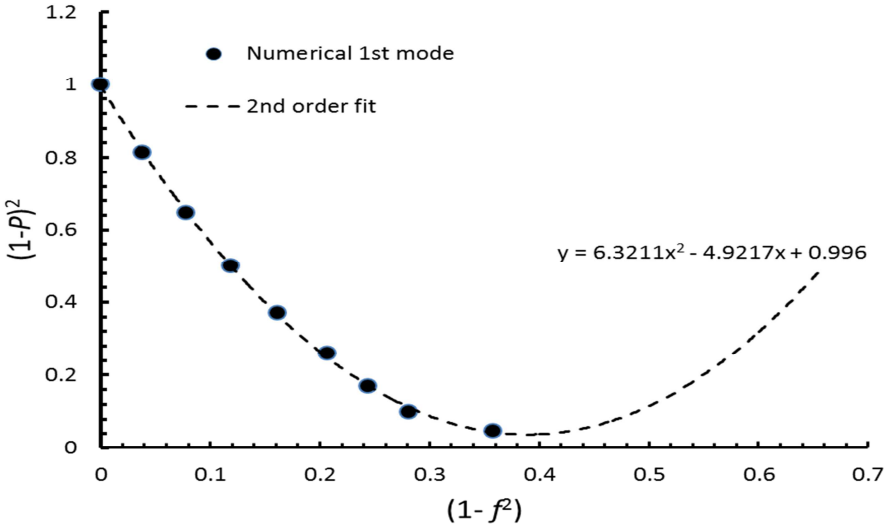

Fig. 12. Second VCT approach (Proposed by Arbelo et al. [31, 32]) for CLSC.

Table 6 Buckling load estimation using the VCT approach.

Parameter	Value
Percent of the applied load ($p \times 100$)	78.1
Second order equation	$y = 6.3211x^2 - 4.9217x + 0.996$
ξ^2	0.0379
P_{VCT}	41.22 kN

7.3. *Results of nonlinear buckling analysis*

Here, the nonlinear buckling load of the imperfect CLSC structure was calculated using the Riks method. By implementing this method, the load proportionally factor (LPF) was 0.825, and the nonlinear buckling load P_{Non} was 42.26 kN.

Besides, the nonlinear numerical and experimental buckling mode shapes are shown in Fig. 13. As can be seen, the mode shapes are almost identical. Consequently, it can be remarked that the nonlinear FE model has the ability to estimate the buckling load with high accuracy.

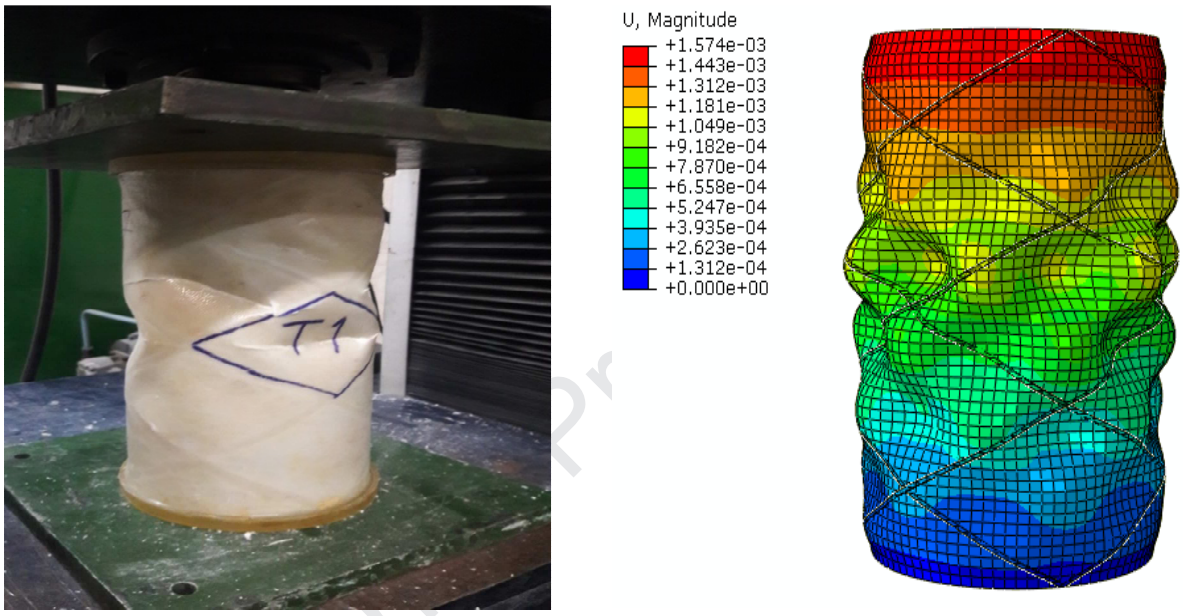

(a) (b)

Fig. 13. (a) Experimental and (b) nonlinear buckling mode shapes of the CLSC.

7.4. *Validation of VCT and comparison between obtained results*

Table 7 presents a comparison between the experimental buckling load P_{EXP}, the predicted buckling load using the VCT approach P_{VCT}, and nonlinear buckling load P_{Non}, with the respective deviations δ (related to the experimental buckling load P_{EXP}). The results corroborate that the difference between P_{VCT} and P_{Non} with P_{EXP} is 2.36% and 4.94%, respectively. Furthermore, the difference between P_{VCT} and P_{Non} is 2.52 %. From the obtained results, it is clear that there is a considerable agreement between the predicted buckling load using the VCT and the experimental and nonlinear buckling loads. Additionally, the VCT result is much more accurate than the nonlinear result. Besides, the maximum applied load level is 78.1% of the linear buckling load, therefore, it can be confirmed that the VCT approach could be considered as a truly non-destructive method to estimate the buckling load of CLSC structures with appropriate accuracy.

Table 7 Comparison of predicted and experimental buckling loads.

Parameter	Value [kN]	δ [%]
P_{EXP}	40.27	---
P_{VCT}	41.22	2.36
P_{Non}	42.26	4.94

7.5. *The effect of maximum applied load (P_{MAX}) on VCT results*

The maximum applied load ($P_{\mathrm{MAX}} = \frac{P_{\mathrm{a}}}{P_{\mathrm{EXP}}} \times 100$) has a great influence on the accuracy of the VCT method. P_{MAX} shows the validity, reliability, and applicability of the VCT approach. This parameter is different for different structures and its optimal value must be obtained. It was investigated considering 50%, 80%, 68%, 67%, 50%, and 81.76% for stringer stiffened curved panels [33], unstiffened cylindrical shell [35], grid-stiffened composite cylindrical shell [57], composite sandwich plates with iso-grid cores [39], isotropic cylindrical shells [38], and unstiffened composite cylindrical shells [36], respectively. The authors proved that the VCT approach achieved a very good correlation when the mentioned maximum load applied to the structures. Consequently, the main goal of this section is to obtain the reasonable maximum applied load of CLSC. For this purpose, four maximum applied loads, specifically,15, 20, 25, and 30 kN are selected. These applied loads are 37.2%, 49.7%, 62.1% and 74.5% of the experimental buckling load, respectively. As shown in Fig. 14, ξ^2 is calculated based on a second-order equation adjusted in the characteristic chart $(1-p)^2$ versus $(1-f^2)$ for the considered axially applied loads; accordingly, these results are reported in Table 8. Furthermore, the corresponding predicted buckling loads for these four maximum applied loads are also reported in Table 8. From the above-mentioned results, it can be seen that the proposed approach has a good correlation with less than 3.15% deviation from the experimental buckling load when P_{MAX} adopted in the VCT is higher than 62.1%. Additionally, the evaluated VCT failed when P_{MAX} is lower than 49.7%.

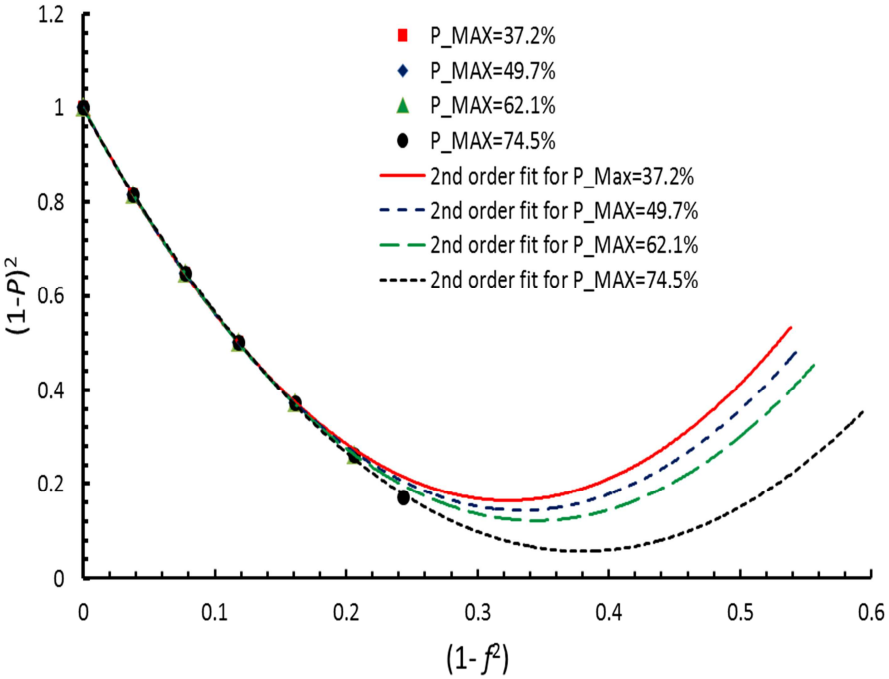

Fig. 14. Calculated ξ^2 for different maximum applied loads.

Table 8 The effect of maximum applied load on the accuracy of the VCT approach.

Maximum applied load (P_a) [kN]	P_{MAX}[%]	ξ^2	P_{VCT} [kN]	δ [%]
15	37.2	0.1640	30.47	24.3
20	49.7	0.1432	31.82	20.9
25	62.1	0.1215	33.35	17.1
30	74.5	0.0567	39.00	3.15

8. Conclusions

In this article, numerical and experimental validations of the VCT approach were presented to predict the buckling load of a CLSC structure under uniaxial loading. Firstly, the general steps for the VCT implementation were presented. The research investigated two VCT approaches, which have been widely used in the literature for imperfection-sensitive structures. Using the FSDT and Rayleigh-Ritz method, the formulation for the vibration of an axially loaded CLSC structure was revisited. Moreover, three types of finite element analyses, which are linear buckling and free vibration, nonlinear free vibration of axially loaded, and nonlinear buckling analyses, are performed. At first, the critical buckling load and first natural frequency for different load levels are calculated and compared to the analytical results for validation of the numerical models. Then, the FE model considering geometric nonlinearities and initial imperfection were considered to compute the variation of the first natural frequency with the axially applied load. Besides, the nonlinear buckling analysis is also performed using the Riks

method for a better comparison of the VCT results. Finally, four specimens were built using a silicone rubber mold, and a filament-winding tool. As well, the buckling test was carried out to validate the results of the VCT approach. The main findings of this article are highlighted below:

1-The calculated buckling load using the VCT approach, nonlinear Riks method, and experimental test are 41.22, 42.26, and 40.27 kN, respectively. From the obtained results, there is a very good agreement between VCT results with nonlinear and experimental results. It can be remarked that the VCT approach could be considered as a truly non-destructive method to predict the buckling load of a CLSC structure with appropriate accuracy. As well, considering the experimental results of the CLSC structure tested, the VCT result is much more accurate than the nonlinear Riks result.
2- The evaluated VCT approach has a good estimation when the CLSC structure has been loaded up to at least 62.1% of the experimental buckling load.
3- The maximum difference between analytical and numerical results for the perfect CLSC structure is less than 1.1%. It can be concluded that the analytical approach has a high accuracy to represent the behavior of loaded perfect CLSC structure. It should be noted that the mentioned approach could be developed for imperfection-sensitive CLSC structure in future works.
4- The first VCT approach, which has been presented by Souza et al. [40, 41], is unable to predict the critical buckling load of CLSC.

9. References

[1] Meyer R., Harwood, O., Harmon, M., Orlando, J., “Isogrid design handbook “, 1973.
[2] Vasiliev V., Barynin, V., Rasin, A., “Anisogrid lattice structures–survey of development and application “, Composite structures, Vol. 54, No. 2, pp. 361-370, 2001.
[3] Vasiliev V., Razin, A., “Anisogrid composite lattice structures for spacecraft and aircraft applications “, Composite structures, Vol. 76, No. 1, pp. 182-189, 2006.
[4] Shahgholian-Ghahfarokhi D., Rahimi, G., “New analytical approach for buckling of composite sandwich pipes with iso-grid core under uniform external lateral pressure “, Journal of Sandwich Structures & Materials, pp. 1099636218821397, 2019.
[5] Hashemian R., Mohareb, M., “Finite difference model for the buckling analysis of sandwich pipes under external pressure “, Ocean Engineering, Vol. 122, pp. 172-185, 2016.
[6] Morozov E., Lopatin, A., Nesterov, V., “Finite-element modelling and buckling analysis of anisogrid composite lattice cylindrical shells “, Composite Structures, Vol. 93, No. 2, pp. 308-323, 2011.
[7] Fan H., Fang, D., Chen, L., Dai, Z., Yang, W., “Manufacturing and testing of a CFRC sandwich cylinder with Kagome cores “, Composites Science and Technology, Vol. 69, No. 15, pp. 2695-2700, 2009.
[8] Buragohain M., Velmurugan, R., “Study of filament wound grid-stiffened composite cylindrical structures “, Composite Structures, Vol. 93, No. 2, pp. 1031-1038, 2011.
[9] Vasiliev V. V., Barynin, V. A., Razin, A. F., “Anisogrid composite lattice structures–Development and aerospace applications “, Composite structures, Vol. 94, No. 3, pp. 1117-1127, 2012.
[10] Sun F., Fan, H., Zhou, C., Fang, D., “Equivalent analysis and failure prediction of quasi-isotropic composite sandwich cylinder with lattice core under uniaxial compression “, Composite Structures, Vol. 101, pp. 180-190, 2013.
[11] Chen L., Fan, H., Sun, F., Zhao, L., Fang, D., “Improved manufacturing method and mechanical performances of carbon fiber reinforced lattice-core sandwich cylinder “, Thin-Walled Structures, Vol. 68, pp. 75-84, 2013.
[12] Han Y., Wang, P., Fan, H., Sun, F., Chen, L., Fang, D., “Free vibration of CFRC lattice-core sandwich cylinder with attached mass “, Composites Science and Technology, Vol. 118, pp. 226-235, 2015.

[13] Lopatin A., Morozov, E., Shatov, A., "Buckling and vibration of composite lattice elliptical cylindrical shells ", Proceedings of the Institution of Mechanical Engineers, Part L: Journal of Materials: Design and Applications, Vol. 233, No. 7, pp. 1255-1266, 2019.
[14] Jiang S., Sun, F., Fan, H., Fang, D., "Fabrication and testing of composite orthogrid sandwich cylinder ", Composites Science and Technology, Vol. 142, pp. 171-179, 2017.
[15] Jiang S., Sun, F., Fan, H., "Multi-failure theory of composite orthogrid sandwich cylinder ", Aerospace Science and Technology, Vol. 70, pp. 520-525, 2017.
[16] Sun F., Lai, C., Fan, H., "Failure mode maps for composite anisogrid lattice sandwich cylinders under fundamental loads ", Composites Science and Technology, Vol. 152, pp. 149-158, 2017.
[17] Shahgholian-Ghahfarokhi D., Rahimi, G., "An analytical approach for global buckling of composite sandwich cylindrical shells with lattice cores ", International Journal of Solids and Structures, 2018.
[18] Shahgholian-Ghahfarokhi D., Rahimi, G., "Buckling analysis of composite lattice sandwich shells under uniaxial compression based on the effective analytical equivalent approach ", Composites Part B: Engineering, pp. 106932, 2019.
[19] Shahgholian-Ghahfarokhi D., Rahimi, G., "A Sensitivity Study of the Free Vibration of Composite Sandwich Cylindrical Shells with Grid Cores ", Iranian Journal of Science and Technology, Transactions of Mechanical Engineering, September 03, 2018.
[20] Sommerfeld A., "Eine einfache Vorrichtung zur Veranschaulichung des Knickungsvorganges ", Zeitschrift des Verein Deutscher Ingenieure (ZVDI), pp. 1320-1323, 1905.
[21] Chu T., "Determination of buckling loads by frequency measurements," Thesis, California Institute of Technology, 1949.
[22] Johnson E., Goldhammer, B., *A Determination of the Critical Load of a Column or Stiffened Panel in Compression by the Vibration Method*, DAVID TAYLOR MODEL BASIN WASHINGTON DC, pp. 1952.
[23] Radhakrishnan R., "Prediction of buckling strengths of cylindrical shells from their natural frequencies ", Earthquake Engineering & Structural Dynamics, Vol. 2, No. 2, pp. 107-115, 1973.
[24] Chailleux A., Hans, Y., Verchery, G., "Experimental study of the buckling of laminated composite columns and plates ", International Journal of Mechanical Sciences, Vol. 17, No. 8, pp. 489-IN2, 1975.
[25] Jubb J., Phillips, I., Becker, H., "Interrelation of structural stability, stiffness, residual stress and natural frequency ", Journal of Sound and Vibration, Vol. 39, No. 1, pp. 121-134, 1975.
[26] Singer J., Abramovich, H., "Vibration techniques for definition of practical boundary conditions in stiffened shells ", AIAA Journal, Vol. 17, No. 7, pp. 762-769, 1979.
[27] Plaut R. H., Virgin, L. N., "Use of frequency data to predict buckling ", Journal of Engineering Mechanics, Vol. 116, No. 10, pp. 2330-2335, 1990.
[28] Singer J., Arbocz, J., Weller, T., "Buckling experiments: experimental methods in buckling of thin-walled structures. Shells, built-up structures, composites and additional topics: Wiley Online Library, 2002.
[29] Sukajit P., Singhatanadgid, P., Identification of buckling load of thin plate using the vibration correlation technique, in *Proceeding of*, 17-19.
[30] Singhatanadgid P., Sukajit, P., Determination of buckling load of rectangular plates using measured vibration data, in *Proceeding of*, International Society for Optics and Photonics, pp. 73753Z.
[31] Arbelo M. A., de Almeida, S. F., Donadon, M. V., Rett, S. R., Degenhardt, R., Castro, S. G., Kalnins, K., Ozoliņš, O., "Vibration correlation technique for the estimation of real boundary conditions and buckling load of unstiffened plates and cylindrical shells ", Thin-Walled Structures, Vol. 79, pp. 119-128, 2014.
[32] Arbelo M. A., Kalnins, K., Ozolins, O., Skukis, E., Castro, S. G., Degenhardt, R., "Experimental and numerical estimation of buckling load on unstiffened cylindrical shells using a vibration correlation technique ", Thin-Walled Structures, Vol. 94, pp. 273-279, 2015.
[33] Abramovich H., Govich, D., Grunwald, A., "Buckling prediction of panels using the vibration correlation technique ", Progress in Aerospace Sciences, Vol. 78, pp. 62-73, 2015.
[34] Chaves-Vargas M., Dafnis, A., Reimerdes, H.-G., Schröder, K.-U., "Modal parameter identification of a compression-loaded CFRP stiffened plate and correlation with its buckling behaviour ", Progress in Aerospace Sciences, Vol. 78, pp. 39-49, 2015.
[35] Skukis E., Ozolins, O., Kalnins, K., Arbelo, M. A., "Experimental test for estimation of buckling load on unstiffened cylindrical shells by vibration correlation technique ", Procedia Engineering, Vol. 172, pp. 1023-1030, 2017.

[36] Franzoni F., Odermann, F., Lanbans, E., Bisagni, C., Arbelo, M. A., Degenhardt, R., "Experimental validation of the vibration correlation technique robustness to predict buckling of unstiffened composite cylindrical shells ", Composite Structures, Vol. 224, pp. 111107, 2019.

[37] Franzoni F., Odermann, F., Wilckens, D., Skuķis, E., Kalniņš, K., Arbelo, M. A., Degenhardt, R., "Assessing the axial buckling load of a pressurized orthotropic cylindrical shell through vibration correlation technique ", Thin-Walled Structures, Vol. 137, pp. 353-366, 2019.

[38] Franzoni F., Degenhardt, R., Albus, J., Arbelo, M. A., "Vibration correlation technique for predicting the buckling load of imperfection-sensitive isotropic cylindrical shells: An analytical and numerical verification ", Thin-Walled Structures, Vol. 140, pp. 236-247, 2019.

[39] Shahgholian-Ghahfarokhi D., Aghaei-Ruzbahani, M., Rahimi, G., "Vibration correlation technique for the buckling load prediction of composite sandwich plates with iso-grid cores ", Thin-Walled Structures, Vol. 142, pp. 392-404, 2019.

[40] Souza M., Fok, W., Walker, A., "Review of Experimental Techniques for Thin-walled Structures Liable to Buckling: Neutral and Unstable Buckling ", experimental techniques, Vol. 7, No. 9, pp. 21-25, 1983.

[41] Souza M., Assaid, L., "A new technique for the prediction of buckling loads from nondestructive vibration tests ", Experimental Mechanics, Vol. 31, No. 2, pp. 93-97, 1991.

[42] Skukis E., Ozolins, O., Andersons, J., Kalnins, K., Arbelo, M. A., "Applicability of the Vibration Correlation Technique for Estimation of the Buckling Load in Axial Compression of Cylindrical Isotropic Shells with and without Circular Cutouts ", Shock and Vibration, Vol. 2017, 2017.

[43] Shahgholian-Ghahfarokhi D., Rahimi, G., "Buckling load prediction of grid-stiffened composite cylindrical shells using the vibration correlation technique ", Composites Science and Technology, Vol. 167, pp. 470-481, 2018.

[44] Labans E., Abramovich, H., Bisagni, C., "An experimental vibration-buckling investigation on classical and variable angle tow composite shells under axial compression ", Journal of Sound and Vibration, Vol. 449, pp. 315-329, 2019.

[45] Tahani V., Shahgholian-Ghahfarokhi, D., Rahimi, G., "Experimental and numerical investigation of effect of shape of ribs on flexural behavior of grid composite plates ", Modares Mechanical Engineering,, Vol. 16, No. 6, pp. 303-311, 2016.

[46] Reddy J. N., "Mechanics of laminated composite plates and shells: theory and analysis: CRC press, 2004.

[47] Kidane S., Li, G., Helms, J., Pang, S.-S., Woldesenbet, E., "Buckling load analysis of grid stiffened composite cylinders ", Composites Part B: Engineering, Vol. 34, No. 1, pp. 1-9, 2003.

[48] Xu Y., Tong, Y., Liu, M., Suman, B., "A new effective smeared stiffener method for global buckling analysis of grid stiffened composite panels ", Composite Structures, Vol. 158, pp. 83-91, 2016.

[49] Vinson J. R., Sierakowski, R. L., "The behavior of structures composed of composite materials: Springer Science & Business Media, 2006.

[50] Dong Y., Li, Y., Chen, D., Yang, J., "Vibration characteristics of functionally graded graphene reinforced porous nanocomposite cylindrical shells with spinning motion ", Composites Part B: Engineering, Vol. 145, pp. 1-13, 2018.

[51] Yang J., Chen, D., Kitipornchai, S., "Buckling and free vibration analyses of functionally graded graphene reinforced porous nanocomposite plates based on Chebyshev-Ritz method ", Composite Structures, Vol. 193, pp. 281-294, 2018.

[52] Castro S. G., Zimmermann, R., Arbelo, M. A., Khakimova, R., Hilburger, M. W., Degenhardt, R., "Geometric imperfections and lower-bound methods used to calculate knock-down factors for axially compressed composite cylindrical shells ", Thin-Walled Structures, Vol. 74, pp. 118-132, 2014.

[53] Tafreshi A., Bailey, C. G., "Instability of imperfect composite cylindrical shells under combined loading ", Composite Structures, Vol. 80, No. 1, pp. 49-64, 2007.

[54] Gibson R. F., "Principles of composite material mechanics: CRC press, 2016.

[55] Li W., Sun, F., Wang, P., Fan, H., Fang, D., "A novel carbon fiber reinforced lattice truss sandwich cylinder: fabrication and experiments ", Composites Part A: Applied Science and Manufacturing, Vol. 81, pp. 313-322, 2016.

[56] Virgin L. N., "Vibration of axially-loaded structures: Cambridge University Press, 2007.

[57] Shahgholian-Ghahfarokhi D., Aghaei-Ruzbahani, M., rahimi, G., "Prediction of the critical buckling load of grid-stiffened composite plates using Vibration Correlation Technique ", Amirkabir Journal of Mechanical Engineering, Vol. 50, No. 7, pp. 1-10, 2019.

Conflict of Interest:

The authors declare that they have no conflict of interest

Ethical Statement:

The authors declare that have considered ethical standards, and the paper is compliance with ethical standards

Funding Body:

The authors declare that they have no funding Body.

Acknowledgements:

The authors declare that they have no acknowledgements.